

Interactive segmentation in aerial images: a new benchmark and an open access web-based tool

Zhe Wang¹, Shoukun Sun², Xiang Que^{1,3,*}, Xiaogang Ma¹

1. Department of Computer Science, University of Idaho, Moscow, ID 83844, USA

2. Department of Computer Science, University of Idaho, Idaho Falls, ID 83401, USA

3. College of Computer and Information Sciences, Fujian Agriculture and Forestry University, Fuzhou, 350002, China

* Corresponding Author

Abstract:

In recent years, deep learning has emerged as a powerful approach in remote sensing applications, particularly in segmentation and classification techniques that play a crucial role in extracting significant land features from satellite and aerial imagery. However, only a limited number of papers have discussed the use of deep learning for interactive segmentation in land cover classification tasks. In this study, we aim to bridge the gap between interactive segmentation and remote sensing image analysis by conducting a benchmark study on various deep learning-based interactive segmentation models. We assessed the performance of five state-of-the-art interactive segmentation methods (SimpleClick, FocalClick, Iterative Click Loss (ICL), Reviving Iterative Training with Mask Guidance for Interactive Segmentation (RITM), and Segment Anything (SAM)) on two high-resolution aerial imagery datasets. To enhance the segmentation results without requiring multiple models, we introduced the Cascade-Forward Refinement (CFR) approach, an innovative inference strategy for interactive segmentation. We evaluated these interactive segmentation methods on various land cover types, object sizes, and band combinations in remote sensing. Surprisingly, the popularly discussed method, SAM, proved to be ineffective for remote sensing images. Conversely, the point-based approach used in the SimpleClick models consistently outperformed the other methods in all experiments. Building upon these findings, we developed a dedicated online tool called RSISeg for interactive segmentation of remote sensing data. RSISeg incorporates a well-performing interactive model, fine-tuned with remote sensing data. Additionally, we integrated the SAM model into this tool. Compared to existing interactive segmentation tools, RSISeg offers strong interactivity, modifiability, and adaptability to remote sensing data.

Keywords: Interactive segmentation; Deep learning; Land cover classification

1. Introduction:

Remote sensing techniques have experienced rapid development and have become invaluable tools in various fields [1]–[4], as they allow for the collection of large amounts of data across wide areas and over long periods [5]. Remote sensing imagery, with its capability of mapping land cover and land use (LULC), and identifying urban development patterns, provides accurate and effective solutions for environmental monitoring, resource management, and urban planning [6], [7]. Analyzing remote sensing images, nonetheless, poses exceptional challenges due to their high dimensionality, complex spectral character, and spatial variability [8].

In recent years, deep learning has emerged as a powerful approach in remote sensing applications [4], [9], [10]. Leveraging its capability to automatically learn hierarchical representations from large-scale datasets, deep learning has demonstrated remarkable performance in tasks such as land use and land cover classification [10]–[12]. Deep learning-based classification models have surpassed traditional machine learning methods in terms of accuracy and efficiency, enabling a more detailed and accurate understanding of land surface dynamics and changes. While deep learning has gained significant popularity in remote sensing, interactive image segmentation has remained relatively underexplored in the context of remote sensing image analysis. Interactive image segmentation, through the incorporation of user inputs such as scribbles or bounding boxes, accurately delimits areas of interest or objects within the images [13]. The interactive approaches allow users to guide the segmentation process by providing additional input, such as scribbles or bounding boxes, to refine and improve the segmentation results [14].

Interactive segmentation and classification techniques play a crucial role in extracting significant data from satellite and aerial imagery for remote sensing applications. Traditionally, these methods required user interaction to divide images into coherent areas and classify land cover features. Approaches such as seed selection, region growing, and user feedback were utilized to refine the segmentation and improve classification accuracy [15]–[17]. Ge et al. also developed an interactive segmentation method specifically for high-resolution remote sensing images. Their approach combines hierarchical graph cut algorithms and geodesic distance measures for accurate and interactive segmentation of RGB-D images [18]. However, the advent of deep learning has created new possibilities in remote sensing by incorporating interactive techniques and convolutional neural networks (CNNs)[19].

Deep learning-based interactive image segmentation has been extensively studied in the field of computer vision due to its wide range of applications, including object recognition, image editing, and medical imaging [20]–[22]. In recent years, numerous studies have proposed new approaches and techniques to address the challenges and limitations of interactive segmentation methods. Sofiiuk et al. proposed a feature backpropagating refinement scheme (f-BRS), an interactive segmentation method that optimizes intermediate parameters to reduce computation time while improving accuracy [23]. Sun et al. introduced the Cascade-Forward Refinement with the Iterative Click Loss (CFR-ICL) model, which consists of three components that can improve segmentation quality without increasing the number of user interactions [24]. Chen et al. developed FocalClick, a model that improves efficiency and performance for existing masks [25]. Kirillov et al. released the Segment Anything Model (SAM) capable of accurately segmenting any object within an image using just a single click, and built the largest segmentation dataset to date [26]. Liu et al. proposed SimpleClick, an interactive image segmentation method that achieves good segmentation results with a simple implementation [27]. However, the unique characteristics and challenges associated with remote sensing images, such as complex spatial patterns, large-scale coverage, and diverse land cover types, necessitate tailored approaches for interactive segmentation in this domain.

Remote sensing is a critical tool for earth observation, providing valuable insights into land cover, change detection, and semantic segmentation [28]–[30]. To enhance the accuracy and efficiency of analysis, traditional classification and segmentation methods have been widely used in remote sensing. A few papers discussed the concept of ‘interactive’ to unsupervised classification in remote sensing images. Begüm et al. conducted a study on active-learning techniques in batch mode for the interactive classification of remote sensing images [31]. The paper extensively discusses batch selection strategies

and how this approach can improve the efficiency and accuracy of interactive classification in remote sensing. The purpose of utilizing batch-mode active learning in remote sensing image classification is to curtail annotation efforts by selecting batches of informative samples for labeling. In 2013, Jefersson proposed a method for the interactive classification of remote sensing images using multiscale segmentation [32]. This method leveraged boosting-based active learning to select regions at varying scales based on user feedback which led to better classification results than isolated scales. Claudio introduced a new interactive domain-adaption technique utilizing active learning to adapt a supervised classifier trained on one remote sensing image to classify a distinct but related target image [33]. Additionally, Haike et al. presented a change detection technique based on interactive segmentation requiring users to enter labels relevant to the changed and unchanged classes in the different images [34].

Deep learning is emerging as a powerful paradigm in various domains. The deep learning-based interactive segmentation methods allow users to provide feedback to the segmentation algorithm and refine the segmentation outputs, resulting in more accurate and reliable segmentation outcomes. Moreover, interactive segmentation methods can handle challenging cases, such as urban satellite images with complex features, occlusions, and variable lighting conditions [35], which are commonly encountered in remote sensing applications. Therefore, in this paper, we presented a benchmark study of various state-of-the-art interactive segmentation models applied to remote sensing image analysis. We focus on the International Society for Photogrammetry and Remote Sensing (ISPRS) Potsdam and Vaihingen datasets [36], two widely used benchmark datasets in semantic segmentation tasks, which contain high-resolution aerial images with detailed ground truth labels for various land cover classes [37]. Furthermore, we highlighted the importance of applying deep learning-based interactive segmentation to remote sensing image analysis. The ability to incorporate user interactions into the segmentation process can provide valuable contextual information and enhance the accuracy of land cover classification, urban growth identification, and other remote sensing applications. Finally, the study developed an online tool for the interactive segmentation of remote sensing images based on the experimental findings. This tool enables users to segment land objects using their images.

In conclusion, this paper aims to bridge the gap between interactive segmentation and remote sensing image analysis by conducting a benchmark study on various deep learning-based interactive segmentation models. In this study, our main contributions are:

- (1) We investigated how well the current state-of-the-art interactive segmentation methods perform on two ISPRS datasets.
- (2) We evaluated interactive segmentation methods on diverse land cover types, object sizes, and band combinations in remote sensing.
- (3) We developed a novel online tool for interactive segmentation using remote-sensing images based on the findings from the experiments and further compared our tool with the SAM model.

2. Materials and methods

2.1 Dataset

ISPRS Potsdam dataset is a high-resolution aerial imagery dataset designed for semantic labeling and object detection tasks [36]. The dataset covers a 42.4-hectare urban area in Potsdam, Germany, and

comprises several gigabytes of red (R), green (G), blue (B), and near-infrared (IR) imagery. The images have a spatial resolution of 5 cm per pixel and include six labeled object classes such as roads, buildings, trees, and cars. The dataset has been widely used by researchers in the fields of computer vision and remote sensing to benchmark and evaluate algorithms for semantic segmentation and object detection.

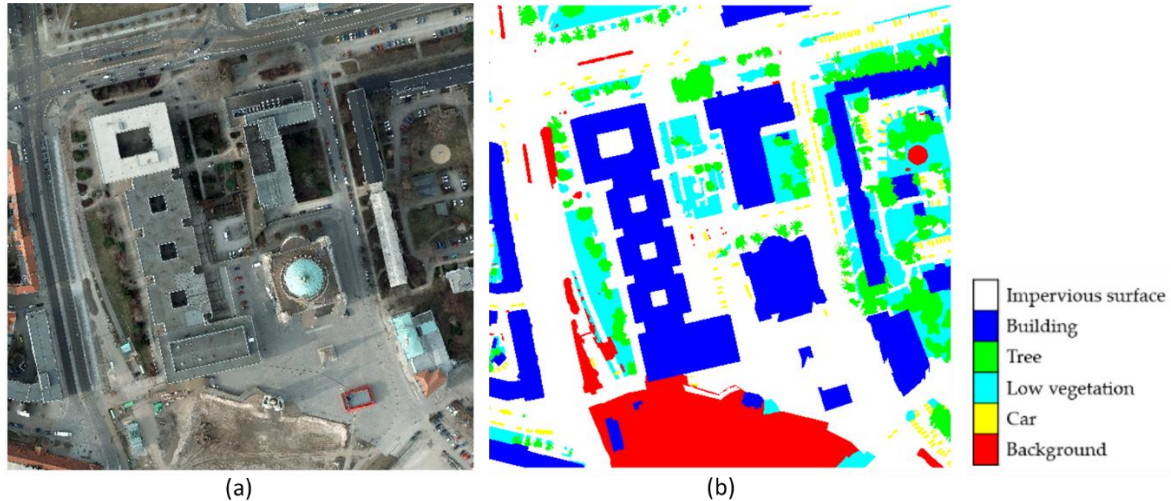


Figure 1. Example patch of Potsdam Dataset; (a) RGB image and (b) labeling image

The ISPRS Vaihingen dataset is a benchmark dataset for semantic labeling and object detection in high-resolution aerial images[36]. It covers a 16 km² area in the town of Vaihingen, Germany, and consists of high-resolution imagery with a spatial resolution of 9 cm per pixel. All images contain three bands, R, G, and IR. The dataset includes five object classes and one background class, such as buildings, trees, roads, and cars, and has been widely used by researchers in the fields of computer vision and remote sensing to develop and evaluate algorithms for semantic segmentation and object detection. The use of this dataset has led to significant advances in the field of computer vision and has enabled the development of more accurate and efficient algorithms for analyzing high-resolution aerial imagery.

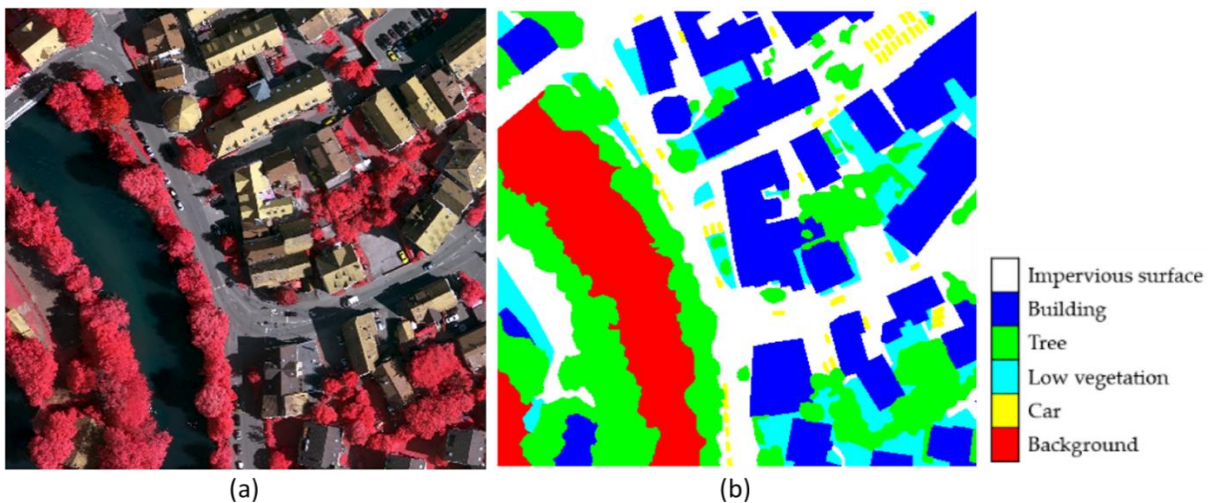


Figure 2. Example patch of Vaihingen Dataset; (a) RGIR image and (b) labeling image

Based on these two datasets, we remade them into four datasets with different band combinations, PRGB (Potsdam RGB), PRGIR (Potsdam RGIR), PRGBIR (Potsdam RGBIR) and VRGIR (Vaihingen RGIR).

2.2 Experiment setup

We undertook the evaluation of models by harnessing the potential of all four datasets (PRGB, PRGIR, PRGBIR and VRGIR). The Potsdam dataset contains 38 images, each image featuring four bands (R, G, B, IR). Of the 38 images, we selected 32 for training, leaving 6 for testing. Every image carries a pixel size of 6000x6000 and a spatial resolution measure of 5 cm. The Vaihingen dataset comes with 33 images: 27 for training and the remaining 6 for testing. Each Vaihingen image has an approximate size of 2000x2500 pixels with 9cm of spatial resolution. Both datasets possess six shared common classes.

As these two datasets are semantic segmentation datasets, we revisited both datasets and morphed them into instance segmentation datasets. This was achieved through a process: each image was broken down into patches and every continuous label belonging to a specific class within a patch was transformed into an object. The Potsdam dataset was broken down into patches of 600x600-pixel size each. The aftermath of this transformation left the training dataset containing 3200 patches and 47152 objects, while the testing dataset featured 600 patches and 10365 objects. With regards to the Vaihingen dataset, after its transformation, we ended up with a training dataset that has 1770 patches and 20102 objects, and a testing dataset of 385 patches and 4651 objects.

For pre-trained models, we conducted testing using the weights and code released by the authors. For fine-tuned models, we trained them using the hyperparameters provided by the authors in the original article.

2.3 Representable models

In interactive segmentation, common interaction methods often include point-based, bounding box, freehand, and scribble interaction. Point-based interaction has several practical advantages in interactive segmentation.

Point-based interaction in interactive segmentation offers precision and efficiency. The specific localization of points allows users to pinpoint areas of interest accurately, resulting in precise segmentation. It's efficient due to minimal interaction cost, requiring only a few clicks or keypresses. This makes it ideal for users to review and refine segmentation results in a feedback loop, allowing prompt corrections or improvements.

2.3.1 FocalClick [25]

Chen et al. proposed the FocalClick method, which utilizes local region prediction and updating of masks to enhance efficiency and performance. FocalClick decomposes slow predictions over the entire image into two fast inferences on small-sized crops: coarse segmentation on target crops and fine refinement on focal crops. The model also introduces the Interactive Mask Correction subtask and presents a strategy called Stepwise Merging as the solution. FocalClick demonstrates improved efficiency and performance, specifically in correcting existing masks.

2.3.2 SimpleClick [27]

Liu et al. proposed SimpleClick, which is a straightforward interactive image segmentation approach that utilizes a plain Vision Transformer pre-trained with mask autoencoders as the backbone network. The approach maintains a single-scale representation through the final layer and generates the final segmentation output through a simple feature pyramid. SimpleClick achieves desirable results in widely used datasets, demonstrating a new application of non-hierarchical, plain Vision Transformers in interactive segmentation, which can also be useful for other dense prediction tasks.

2.3.3 f-BRS [23]

Sofiuk et al. proposed f-BRS, which is an interactive segmentation method that optimizes intermediate parameters to reduce computation time while improving accuracy. The method introduces small variations to achieve consistency between user clicks and segmentation results, which reduces the computational cost of the entire neural network. The experiments showed that this method has achieved better results with faster runtime compared to other existing methods.

2.3.4 Reviving Iterative Training with Mask Guidance for Interactive Segmentation (RITM) [38]

Sofiuk et al. proposed a simple feedforward model and training strategy for point-based interactive segmentation, which utilizes segmentation masks from previous steps and can be restarted during iterative training to allow the network to understand masks from the previous step. The results show that the model trained on a combined dataset of COCO and LVIS achieves the best performance. Additionally, the proposed method is expanded to allow for modifying existing instance segmentation masks, providing new directions for the design of interactive segmentation. The paper provides an in-depth introduction to the history, related work, proposed method, and experimental results of interactive segmentation.

2.3.5 ICL-CFR [24]

Sun et al. introduced the ICL-CFR model, which is an interactive image segmentation approach comprising three new components CFR, ICL, and SUEM image enhancement. ICL is a new training strategy that defines the model preference of using fewer users, and SUEM is a new data augmentation technique. The model exhibits promising performance in five commonly used datasets and can improve segmentation quality without increasing user interactivity, surpassing the best results from previous works.

Furthermore, the CFR approach introduces an innovative inference strategy for interactive segmentation that allows for iterative refinement of the segmentation results without the need for multiple models. The proposed CFR method incorporates two inference loops: an outer loop and an inner loop. By combining the outer and inner loops, the CFR approach enables a comprehensive refinement process. The outer loop sets the initial segmentation foundation, while the inner loop further improves the quality and accuracy of the segmentation by iteratively refining the mask using the same model. This iterative refinement strategy eliminates the need for separate models and simplifies the overall segmentation process. By iteratively incorporating user interactions and leveraging the capabilities of the segmentation model, CFR facilitates the generation of more precise and detailed segmentation masks. This methodology enhances the user experience by reducing the effort required for refining the segmentation and ultimately improves the quality of the final segmentation results.

2.3.6 SAM [26]

The SAM developed by Meta AI is an advanced AI model capable of accurately segmenting any object within an image using just a single click. SAM stands out as a promotable segmentation system that can generalize its segmentation capabilities to unfamiliar objects and images without requiring additional training. SAM's exceptional performance is attributed to its extensive training on a large dataset consisting of 11 million images and 1.1 billion masks. This comprehensive training allows SAM to effectively generate masks for all objects present in an image. Alternatively, users have the option to provide specific points or guidance to SAM, enabling the model to generate precise masks tailored to a particular object of interest.

3. Experiments and results

Our experiment was conducted in three steps to evaluate the performance of various interactive segmentation models, comprising a total of five models as mentioned in section 2.3. We improved RITM, and SimpleClick models using Sun's proposed CFR method. The CFR is not applied with FocalClick because it already has a local refinement module. In the first step, we initially evaluated eight models, SimpleClick, SimpleClick-CFR, ICL, ICL-CFR, RITM, RITM-CFR, FocalClick, and SAM. Following this, we fine-tuned and tested the models on remote sensing datasets, Potsdam and Vaihingen, in order to assess their performance. In the initial step, SAM and FocalClick models demonstrated poor performance compared to the other models. Thus, we compared ICL, RITM, SimpleClick, and their CFR modes in the second step. However, it should be noted that all discussed models initially required three-channel input, while the Potsdam dataset images contain four bands. Hence, in the third step, we examined the performance of various interactive segmentation methods with multiple-band combinations and land cover types, including different plot sizes that were under different land cover types. Finally, we selected the SimpleClick model to be the best performer, and we modified its input structure to test its performance on four-band remote sensing data, inputting all four bands.

3.1 Evaluate the models with initial weights.

We evaluated the model performance using the number of clicks (NoC)[23], and the average click number required to reach the target intersection over union (IoU)[39]. It's a measure of how many clicks or interactions a user provides to achieve a desired result. Lower NoC suggests a more efficient model as it requires fewer user interactions for accurate segmentation. The average click number required to reach the target IoU can be found using iterative interaction and segmentation mechanisms. At the start, the model might generate an initial segmentation with low IoU. Then in the next iterations, additional user clicks can be introduced to improve the segmentation until the target IoU is reached. We reported the NoC to achieve the IoU at four levels four evaluation, 80%, 85%, 90%, and 95%, which correspond to the metrics NoC80, NoC85, NoC90, and NoC95 respectively.

Figure 3 illustrates example patches featuring RGB imaging, RGIR imaging, and individual imaging across four separate bands (R, G, B, IR) within the VRGBIR dataset. A RGIR composite image in remote sensing can help make the vegetation appear clearer and more differentiated from other features. This is because it utilizes the near-infrared band, a spectrum to which vegetation strongly responds. Chlorophyll in healthy vegetation absorbs visible light (0.4 - 0.7 μm) for use in photosynthesis, whereas the cell structure of the leaves strongly reflects near-infrared light (0.7 - 1.1 μm). Hence, when viewed in an RGIR composite image (where infrared data is often coded in red), vegetation typically appears bright red, making it easier to identify and examine.

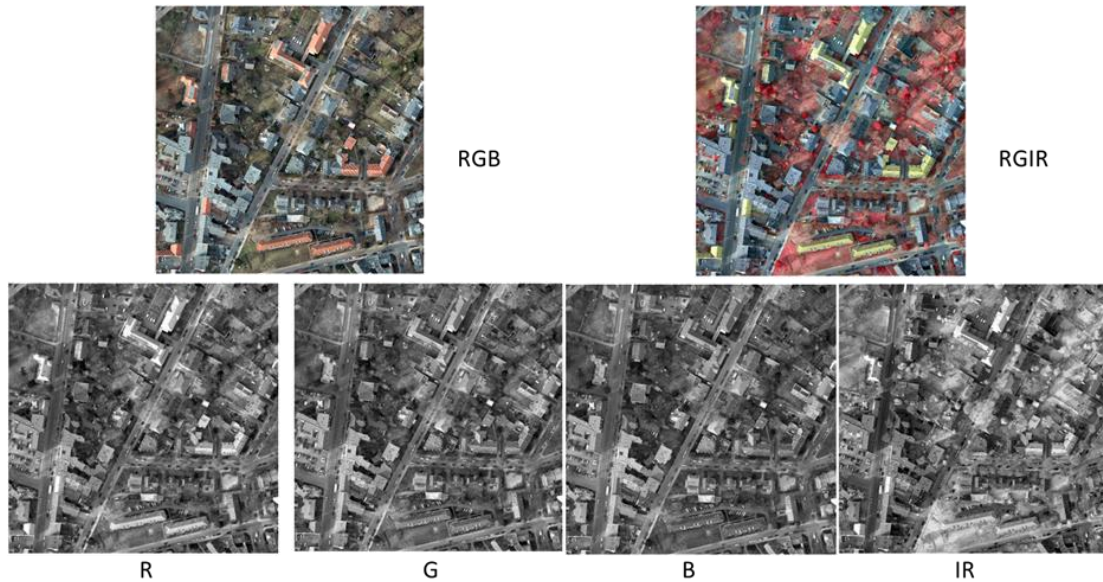


Figure 3. Comparative visualization of RGB, RGIR, R, G, B, and IR imaging

Table 1 shows the performance of different interactive segmentation models on PRGB and PRGIR datasets without finetuning at varying IoU levels. On the PRGB dataset, RITM demonstrates the best performance at the 80% IoU level. The SimpleClick-CFR model performs best at higher IoU levels (85%, 90%, and 95%), demonstrating its ability to achieve finer and more accurate segmentation results. Except for SAM and Focal Click, the remaining models exhibit similar performance at the higher IoU levels (85%, 90%, and 95%). However, it is important to note that as the desired IoU level increases, the efficiency of all models declines significantly. While the least-performing model at the 80% IoU level requires less than seven clicks, at the 95% IoU level, even the best-performing model, SimpleClick-CFR, requires approximately fourteen clicks. This trade-off between precision and efficiency becomes evident at higher IoU thresholds. On the PRGIR dataset, SimpleClick and SimpleClick-CFR consistently demonstrate strong performance across multiple IoU thresholds. SimpleClick requires the fewest number of clicks at 80% IoU, and it maintains its superiority at 85%, 90%, and 95% IoU levels. RITM and RITM-CFR models also exhibit competitive performance across different IoU thresholds. However, SAM consistently requires the highest number of clicks, indicating comparatively lower performance.

Table 1. Evaluation Results on PRGB and PRGIR Dataset without Finetuning

Model Name	PRGB Dataset				PRGIR Dataset			
	NoC80	NoC85	NoC90	NoC95	NoC80	NoC85	NoC90	NoC95
SimpleClick	4.90	6.27	8.84	14.31	4.83	6.45	9.24	14.95
SimpleClick-CFR	4.94	6.26	8.80	14.28	4.90	6.44	9.29	14.83
ICL	5.04	6.47	9.10	14.61	5.10	6.65	9.64	15.24
ICL-CFR	5.14	6.54	9.15	14.62	5.11	6.73	9.63	15.20
RITM	4.78	6.34	9.22	14.89	5.22	6.87	10.00	15.52
RITM-CFR	4.81	6.34	9.23	14.90	5.36	7.08	10.14	15.53
FocalClick	5.56	7.05	9.70	15.01	5.26	6.96	10.04	15.28
SAM	6.58	8.77	12.34	17.54	6.78	9.34	13.36	17.78

Figure 4 reveals the varying trends of mIoU for eight distinct models, as the number of clicks increases from 1 to 10. At the outset, the RITM-CFR model emerges as the most effective with just a single click. As the click count rises from 2 to 4, the performance of the SAM model remains largely consistent and comparable to both RITM and RITM-CFR. Yet, once the click count surpasses 5, SAM persistently registers a slight underperformance relative to the other models. Upon reaching 10 clicks, all models display a mIoU near 0.9, with the sole exception of SAM, which falls short at under 0.85.

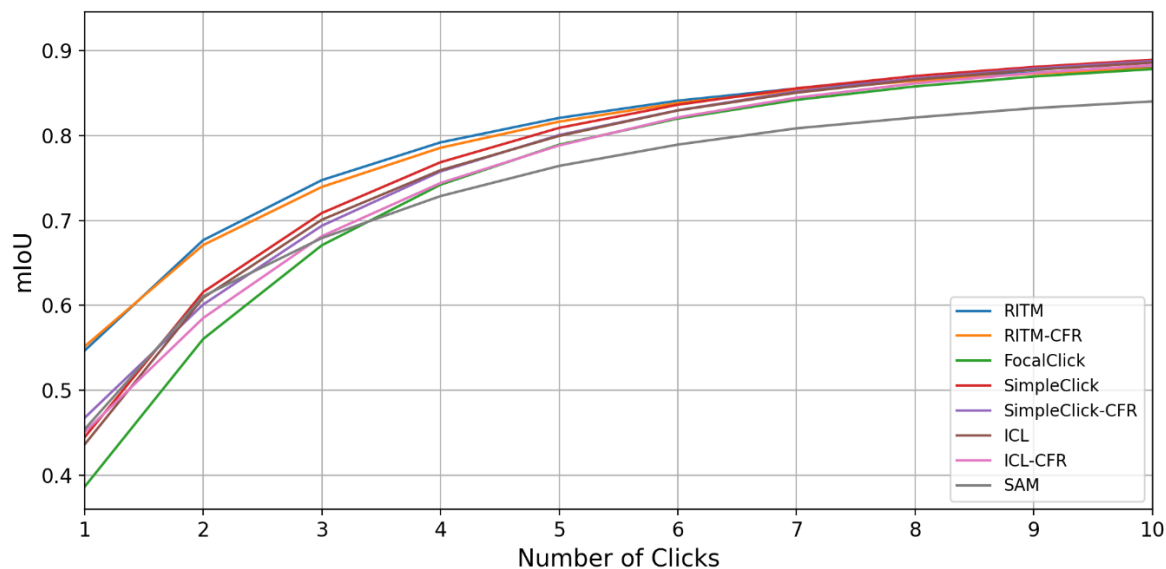


Figure 4. Mean IoU (mIoU) given n clicks (n ranges from 1 to 10) of eight models.

3.2 Evaluate the models after fine-tuning.

Table 2 shows the results of interactive segmentation models after finetuning. SimpleClick and SimpleClick models consistently exhibit superior performance with lower click counts across all IoU thresholds, indicating their remarkable efficiency in user interaction for accurate segmentation. The "ICL" and "ICL-CFR" models exhibit slightly higher click counts, indicating a relatively increased level of user interaction. However, they still deliver reasonable performance with a moderate number of clicks to achieve accurate segmentation results. Similarly, the "RITM" and "RITM-CFR" models present slightly higher click counts but maintain efficient user interaction for achieving accurate segmentations.

Table 2. Evaluation Results on PRGB and PRGIR Dataset after Finetuning

Model Name	PRGB dataset				PRGIR dataset			
	NoC80	NoC85	NoC90	NoC95	NoC80	NoC85	NoC90	NoC95
SimpleClick	3.26	4.39	6.73	12.47	3.30	4.42	6.77	12.45
SimpleClick-CFR	3.28	4.39	6.74	12.45	3.27	4.39	6.77	12.43
ICL	3.70	5.04	7.69	13.61	4.32	5.87	8.90	15.01
ICL-CFR	3.64	4.95	7.59	13.55	4.16	5.73	8.74	14.93

RITM	3.92	5.36	8.18	14.10	4.18	5.67	8.60	14.45
RITM-CFR	3.86	5.30	8.13	14.03	4.16	5.62	8.54	14.36

Figure 5 provides a comparative analysis of the mIoU for models, both fine-tuned and non-fine-tuned, as the number of clicks varies from 1 to 10. With only one click, fine-tuned models already achieve a mIoU exceeding 0.6. As the click count progressively increases, the fine-tuned models consistently outperform their non-fine-tuned counterparts. However, the performance gap, as quantified by the mIoU, between the two types of models steadily narrows. By the point where the click count hits 10, the superior performance of the fine-tuned models, though still discernible, largely approximates that of the non-fine-tuned models, with scores predominantly hovering around 0.9.

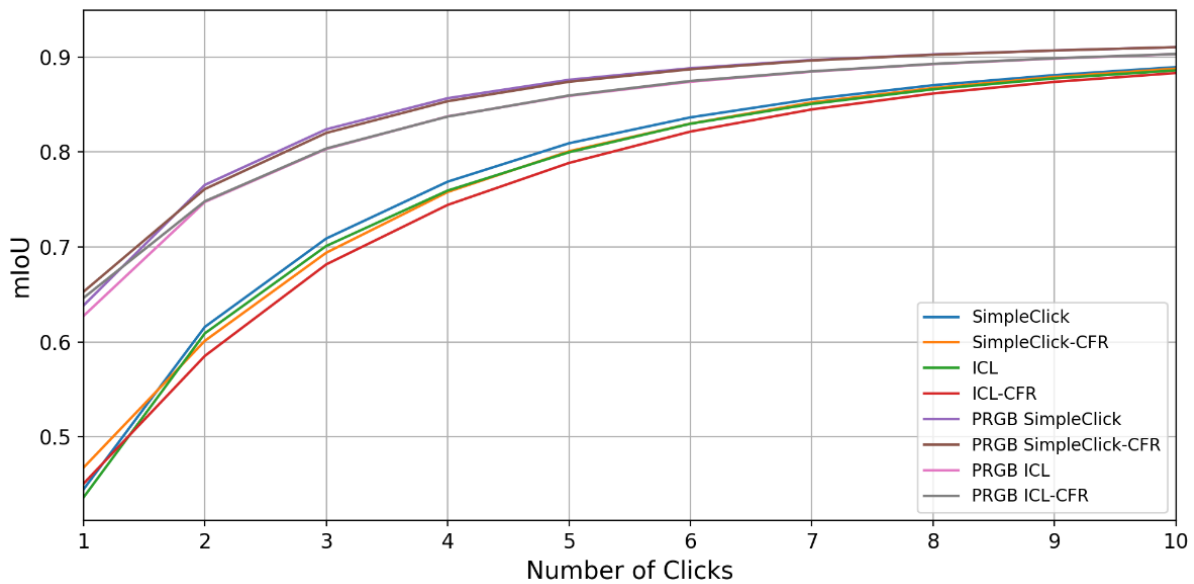


Figure 5. Comparison of mean IoU (mIoU) given n clicks (n ranges from 1 to 10) between models before and after finetuning.

Table 3 demonstrates the evaluation results on the VRGIR dataset before and after finetuning with the PRGIR dataset. Both datasets consist of red, green, and Near-infrared bands. Among the various models we evaluated, the SimpleClick models consistently outperformed the others, achieving superior results across all levels of Intersection over Union (IoU) while requiring a lower number of users' clicks for interactive segmentation. These findings highlight the robustness and efficiency of the SimpleClick models in the context of multispectral data. Moreover, comparing all the models to the baseline model that was not finetuned and directly evaluated on the VRGIR dataset, we observed significant improvements in performance across the board. These results underscore the importance of finetuning models on relevant datasets to enhance their performance on specific tasks, such as interactive segmentation using multispectral imagery.

Table 3. Evaluation Results on VRGIR Dataset Before and After Finetuning with PRGIR Dataset

Model Name	Before finetuning				After finetuning			
	NoC80	NoC85	NoC90	NoC95	NoC80	NoC85	NoC90	NoC95
SimpleClick	4.16	5.70	8.43	14.19	4.83	6.45	9.24	14.95

SimpleClick-CFR	4.16	5.67	8.34	14.22	4.90	6.44	9.29	14.83
ICL	5.24	6.95	10.16	15.72	5.10	6.65	9.64	15.24
ICL-CFR	5.17	6.92	10.21	15.73	5.11	6.73	9.63	15.20
RITM	4.81	6.60	9.65	15.19	5.22	6.87	10.00	15.52
RITM-CFR	4.84	6.47	9.62	15.15	5.36	7.08	10.14	15.53

Figure 5. demonstrates the substantial improvement in model performance when the finetuned models are applied to the VRGIR dataset. Notably, the SimpleClick-CFR model demonstrates the highest level of improvement, exhibiting a remarkable increase of 33.15% at the 80% IoU level. However, it is worth noting that the models show relatively less improvement at the 95% IoU level, suggesting that reaching higher levels of accuracy becomes progressively challenging.

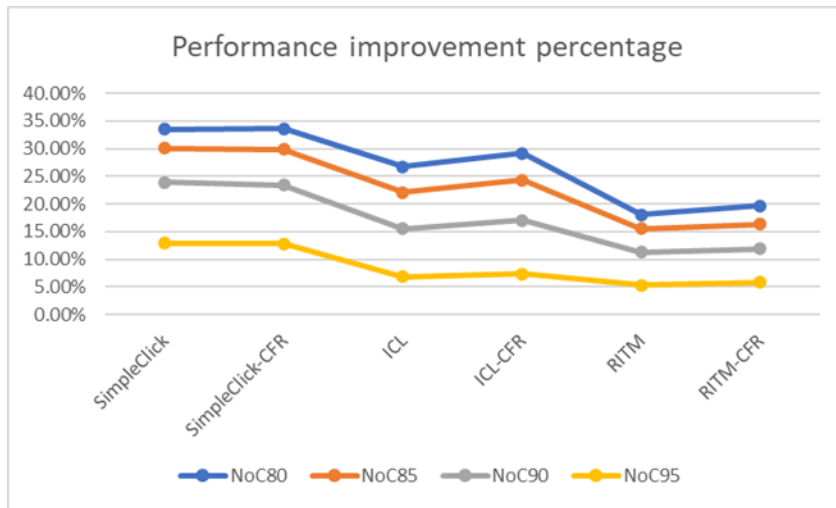


Figure 6. Performance improvement percentage between the modes before and after finetuning.

3.3 Model performance by different classes

Tables 4 and 5 present the results of various interactive segmentation models on several classes, namely: "Impervious Surface," "Building," "Low Vegetation," "Tree," and "Car", respectively. Given that all models exhibit a similar trend in their results, this paper focuses solely on the evaluation performance of the PRGB dataset after finetuning.

Table 4 presents the evaluation results of various interactive segmentation models on the PRGB dataset after fine-tuning. In the SimpleClick model, we observed differing levels of performance across classes. The "Building" class achieved the lowest number of clicks required for accurate segmentation, indicating the model's ability to segment buildings with minimal user input. Conversely, the "Low Vegetation" class presented a greater challenge, with a higher number of clicks required for satisfactory results. The "Tree" class required an intermediate number of clicks, while the "Car" class required a higher number of clicks for successful segmentation. Similar trends were also observed in the SimpleClick-CFR model, with the "Building" class demonstrating the lowest number of clicks (1.83) required for an 80% IoU. For the "Low Vegetation" class, 4.17 clicks were necessary, while the "Tree" class needed 3.27 clicks and the "Car" class required 1.79 clicks for similar IoU levels.

Table 4. Evaluation results by class on the PRGB dataset

Class	Impervious Surface	Building	Low Vegetation	Tree	Car
Model Name	Noc80/95	Noc80/95	Noc80/95	Noc80/95	Noc80/95
SimpleClick	3.53/12.33	1.85/4.63	4.11/13.49	3.22/12.45	1.76/10.45
SimpleClick-CFR	3.55/12.28	1.83/4.69	4.17/13.47	3.27/12.36	1.79/10.46
ICL	4.07/13.67	1.96/5.10	4.77/14.70	3.62/14.16	1.99/11.67
ICL-CFR	3.97/13.62	1.99/5.04	4.70/14.64	3.57/14.07	1.98/11.58
RITM	4.46/14.62	2.30/6.14	4.89/15.22	4.11/14.55	2.09/11.95
RITM-CFR	4.42/14.48	2.31/6.20	4.82/15.07	4.01/14.58	2.01/11.86

Table 5 shows the performance of different interactive segmentation models after finetuning the PRGB dataset. Notably, the observed trend in this table aligns with the patterns observed in Table 4, indicating consistency in the model performances across the evaluated datasets. One intriguing observation is that despite the expected benefits of utilizing the IR band for vegetation segmentation, such as trees and grass, Table 5 reveals a lower efficiency in most classes. This finding suggests that the inclusion of the IR band in the segmentation process may not always lead to improved results, highlighting the complexity and variability of the segmentation task across different land cover classes.

Moreover, consistent with the observations made in Table 1, it is evident that achieving higher IoU levels, particularly at 95%, requires a significantly higher number of clicks. The findings demonstrate that except for the car class, which exhibits a relatively smaller increase, all other classes require approximately three times more clicks to reach the desired IoU level from 80% to 95%. Notably, the car class stands out, necessitating around nine times more clicks, as exemplified by the SimpleClick model, where the click counts increase from 1.85 to 10.40.

Table 5. Evaluation results by class on the PRGIR dataset

Class	Impervious Surface	Building	Low Vegetation	Tree	Car
Model Name	Noc80/95	Noc80/95	Noc80/95	Noc80/95	Noc80/95
SimpleClick	3.55/12.25	1.79/4.68	4.17/13.51	3.14/12.30	1.85/10.40
SimpleClick-CFR	3.55/12.24	1.78/4.67	4.18/13.42	3.12/12.27	1.83/10.48
ICL	4.72/15.10	2.29/6.09	5.56/15.78	4.01/15.56	2.36/14.54
ICL-CFR	4.56/15.11	2.23/5.89	5.40/15.63	3.86/15.55	2.29/14.41
RITM	4.62/15.00	2.51/6.58	5.33/15.47	4.47/15.13	2.19/12.38
RITM-CFR	4.68/14.92	2.52/6.63	5.30/15.38	4.49/15.09	2.16/12.20

3.4 Model performance by different segment sizes

In remote sensing land cover classification, the size of surface objects is a crucial factor [40]. We conducted a further investigation into the relationship between the size of surface objects and the number of clicks required to achieve various IoU thresholds in interactive segmentation. This analysis aimed to gain insights into the impact of object size on the interactive segmentation process and explore

any potential variations in the number of required clicks across different land cover classes at different IoU levels. For our experiments on interactive segmentation, we considered five land cover types, among which the shapes of buildings and trees exhibit relative regularity and variations compared to the other classes. Tables 6 and 7 present the performance of different interactive segmentation models specifically for buildings and trees of varying sizes.

In Table 6, the segment size of the building class was divided into five categories ranging from 0.075 m² to 881.90 m² using the quantile method. Figure 7 shows an example of the different sizes of the building in the images. It is noticeable that larger building segments require fewer clicks to achieve satisfactory IoU levels across the interactive segmentation models. This indicates that the segmentation algorithms are more efficient in dealing with larger building segments than smaller ones. Interestingly, when comparing the building class's performance with other land cover classes, we observed that buildings generally require fewer clicks for successful segmentation. This is attributed to their regular and well-defined shape characteristics, which facilitate the interactive segmentation process, resulting in reduced click requirements for different segment sizes.

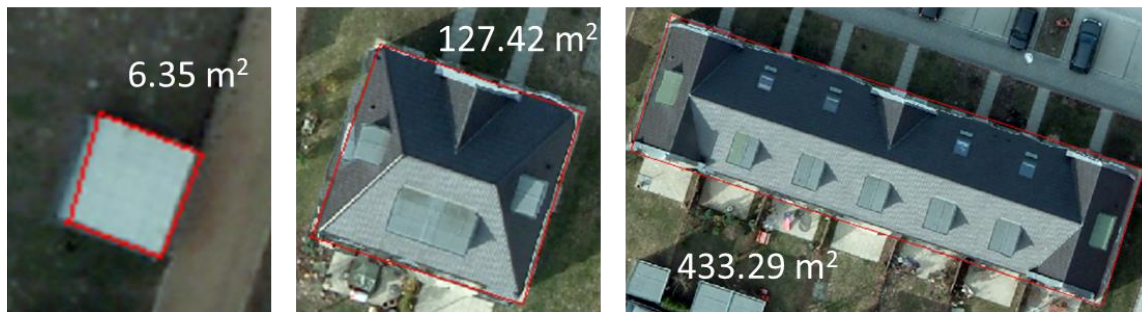


Figure 7. Examples of different sizes of the building segments

Table 6. Building Class Evaluation Results at Various Segment Sizes on the PRGB Dataset

Size	(0.075 m ² , 9.03 m ²]	(9.03 m ² , 36.36 m ²]	(36.36 m ² , 100.08 m ²]	(100.08 m ² , 256.83 m ²]	(256.83 m ² , 881.90 m ²]
Model Name	Noc80/95	Noc80/95	Noc80/95	Noc80/95	Noc80/95
SimpleClick	3.76/12.11	1.483.78	1.36/2.92	1.36/2.25	1.28/2.06
SimpleClick-CFR	3.62/12.36	1.47/3.87	1.37/2.88	1.38/2.28	1.30/2.03
ICL	3.91/12.48	1.63/4.53	1.41/3.38	1.38/2.65	1.44/2.42
ICL-CFR	3.99/12.37	1.63/4.54	1.41/3.27	1.43/2.56	1.48/2.44
RITM	4.09/13.99	1.60/4.76	1.50/3.93	1.68/3.29	2.64/4.72
RITM-CFR	3.83/13.78	1.62/4.76	1.53/4.20	1.80/3.41	2.76/4.81

Table 7 outlines the segment sizes of the tree class, dividing them into five categories using the quantile method, ranging from 0.075 m² to 847.53 m². An intriguing observation is that smaller land objects generally require more clicks to achieve accurate segmentation, a pattern consistent across all evaluated models. This indicates a consistent relationship between object size and the complexity of the segmentation task. Remarkably, the optimal performance in terms of click efficiency is observed within a

specific range of sizes, with the best results obtained for land objects ranging from 155.93 m² to 847.53 m². This suggests that within this size range, interactive segmentation models achieve a favorable balance between accuracy and the number of required clicks, resulting in more efficient and reliable segmentation outcomes.

Table 7. Tree Class Evaluation Results at Various Segment Sizes on PRGB Dataset

Size	(0.075 m ² , 1.96 m ²]	(1.96 m ² , 9.52 m ²]	(9.52 m ² , 37.12 m ²]	(37.12 m ² , 155.93 m ²]	(155.93 m ² , 847.53 m ²]
Model Name	Noc80/95	Noc80/95	Noc80/95	Noc80/95	Noc80/95
SimpleClick	3.55/12.25	1.79/4.68	4.17/13.51	3.14/12.30	1.85/10.40
SimpleClick-CFR	3.55/12.24	1.78/4.67	4.18/13.42	3.12/12.27	1.83/10.48
ICL	4.72/15.10	2.29/6.09	5.56/15.78	4.01/15.56	2.36/14.54
ICL-CFR	4.56/15.11	2.23/5.89	5.40/15.63	3.86/15.55	2.29/14.41
RITM	4.62/15.00	2.51/6.58	5.33/15.47	4.47/15.13	2.19/12.38
RITM-CFR	4.68/14.92	2.52/6.63	5.30/15.38	4.49/15.09	2.16/12.20

3.5 Performance Evaluation with 4-Band Dataset (PRGBIR)

Table 8 displays the models' performance on the PRGBIR dataset, which consists of four bands, offering more spectral information compared to the three-band input. Nevertheless, the results in Table 8 demonstrate that the models trained on the PRGBIR dataset have worse segmentation accuracy and overall performance than those trained on three-band input, as shown in Tables 4 and 5. These findings suggest that despite the inclusion of the additional band, its incorporation does not lead to improved performance. Therefore, it is crucial to carefully consider the impact of additional spectral bands and their relevance to the specific task. Increasing the number of input channels does not necessarily translate into improved performance.

Table 8. Evaluation results on PRGBIR dataset

Model	SimpleClick	SimpleClick-CFR
Class	Noc80/85/90/95	Noc80/85/90/95
Impervious Surface	3.96/5.06/7.50/13.40	3.88/4.98/7.43/13.37
Building	2.00/2.37/3.06/5.02	1.93/2.27/2.93/4.91
Low Vegetation	4.65/6.11/8.80/14.13	4.60/5.95/8.65/14.02
Tree	3.75/4.83/7.09/13.06	3.76/4.82/6.98/13.05
Car	2.03/2.64/4.15/11.18	1.95/2.50/3.83/10.88
Overall	3.72/4.97/7.46/13.11	3.65/4.83/7.30/13.02

4. Interactive Segmentation tool for remote sensing data, RSISeg tool

Drawing on the findings from the above experiments, we developed an online tool, RSISeg for interactive segmentation, specifically tailored to remote sensing imagery. This tool seamlessly integrates models that have been fine-tuned with remote sensing data derived from our earlier experiments, in addition to

incorporating the original SAM model. To optimize its functionality for remote sensing data, the tool is engineered to efficiently process TIFF files and export results in GEOJSON format. This capability considerably simplifies the re-editing process across a range of GIS software platforms.

Figure 8 provides a depiction of the interactive segmentation process in the tool used to delineate land cover objects. The figure demonstrates the use of two types of points: positive clicks and negative clicks. Positive clicks are placed directly on the target land cover segment, indicating the desired area for inclusion within the segment. Conversely, negative clicks are positioned on regions considered irrelevant or not belonging to the intended segment, serving as markers for exclusion.

To maintain the balance between efficiency and accuracy in line with our experimental findings, it is advisable to exercise caution and avoid going beyond 20 clicks for a single land cover segment. Going beyond this limit could decrease the quality and efficiency of segmentation. Therefore, users should exercise caution and provide a reasonable number of clicks within this limit. By adhering to this guideline, users can optimize the interactive segmentation process and achieve a balance between accuracy and the time required for segment delineation.

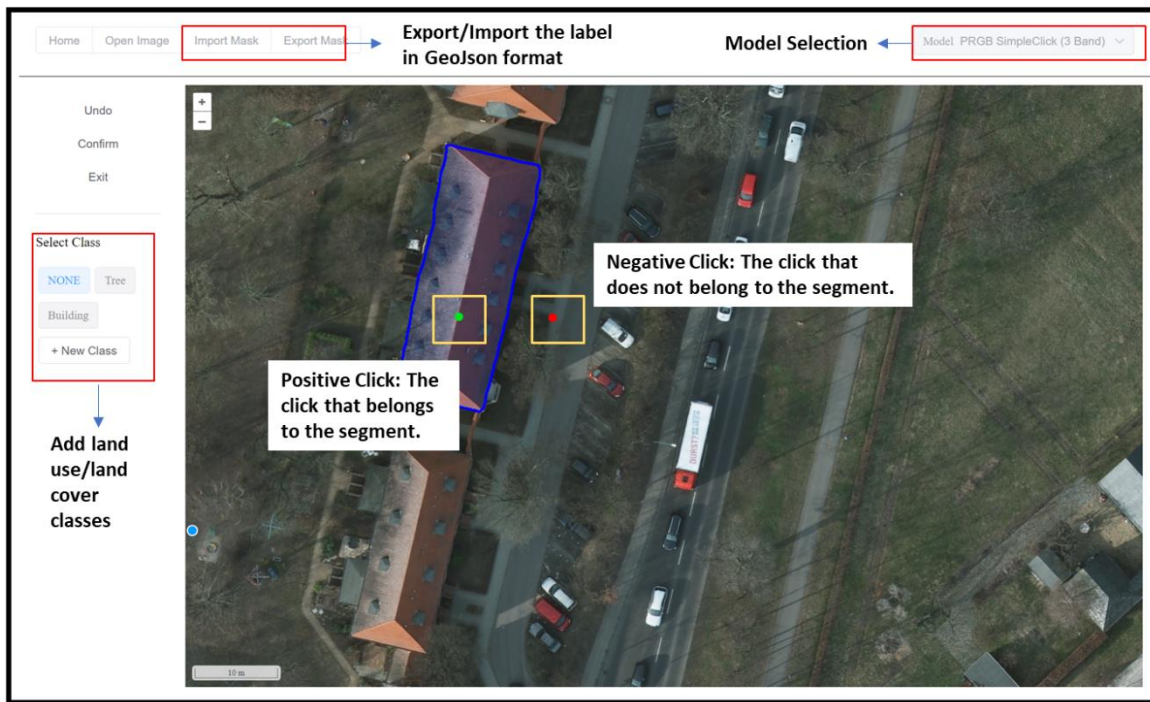


Figure 8. RSISeg user interface screenshot

Figure 9 portrays the end product derived from the interactive segmentation process. The segmented land cover objects generated can be exported in a GeoJSON format, thus facilitating additional analyses and integration with geospatial software, such as QGIS (citation). The tool has two pre-established classes: 'Tree' and 'Building', with the capability for users to append more classifications. As demonstrated in Figure 9, the 'Car' class was additionally added. Moreover, the tool assigns distinct

colors to the different land object classes.



Figure 9. Example interactive segment result

5. Discussion

5.1 Comparison with SAM

In this study, our analysis of different interactive segmentation models has provided valuable insights into their performance and applicability in the field of remote sensing. One notable observation is that the SimpleClick models, namely SimpleClick and SimpleClick-CFR, have consistently exhibited the best performance across various evaluation metrics. These models have showcased their remarkable generalization ability specifically for remote sensing images, even surpassing the performance of the ICL model reported in previous studies on different datasets. This highlights the efficacy and versatility of the SimpleClick models in the context of interactive segmentation tasks within the domain of remote sensing. On the other hand, SAM, which has been trained on an extensive dataset containing a vast number of images and masks, surprisingly displayed the poorest performance among the models evaluated in our study. Despite its large-scale training data, SAM's performance did not match the expectations set by the SimpleClick models. This discrepancy may suggest that the complexity and unique characteristics of remote sensing images require a tailored approach that takes into account specific domain knowledge and considerations.

We have compared SAM and the best model pointed out in this article, SimpleClick, in greater depth. Figure 10 illustrates the process: when segmenting a building, the segmentation results of SAM and SimpleClick with one positive point at the same location, two positive points respectively, as well as the number of points required by the two models to achieve the final segmentation target.

Upon administering a single click, SimpleClick segments an entire building anchored on the clicked location, while SAM only segments half of the building, delineated by the building's ridge. A second click placed on the building's opposite side results in both SimpleClick and SAM sketching out the full building;

however, the edges marked by SAM are noticeably more jagged. Through the addition of negative points to isolate unwanted areas, SimpleClick attains a satisfying segmentation result with just one negative point, equating to a total of three clicks. Conversely, SAM only manages to meet user satisfaction after incorporating several additional points, and the edges of its segmented objects continue to display a level of roughness.

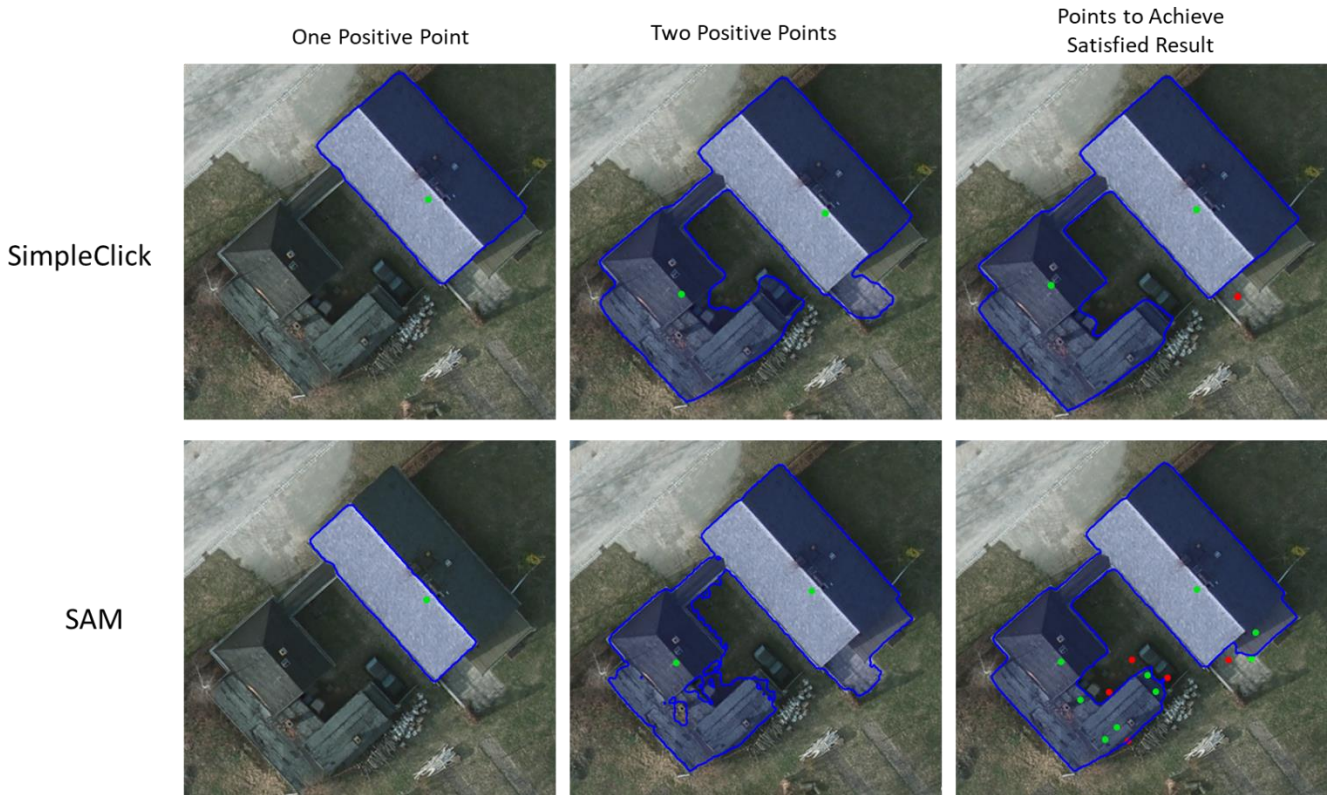


Figure 10. Comparison between SimpleClick and SAM through the process visualization of building segmentation.

Figure 11 displays the percentage of total segments achieving various IoU results for SimpleClick, SimpleClick-CFR, and SAM models when the click count totals 2 and 5. In Figure 11(a), with a click count of 2, all segments with an IoU between 0-0.6 constitute less than 5% of the total. Whereas, for segments with an IoU greater than 0.8, both SimpleClick-CFR and SAM models register a larger count compared to SimpleClick. Moving to Figure 11(b), when the number of clicks increases to 5, the SAM model exhibits the highest segment proportion at an IoU roughly around 0.7. However, when the segments hit an IoU of 0.95, both SimpleClick and SimpleClick-CFR markedly surpass SAM.

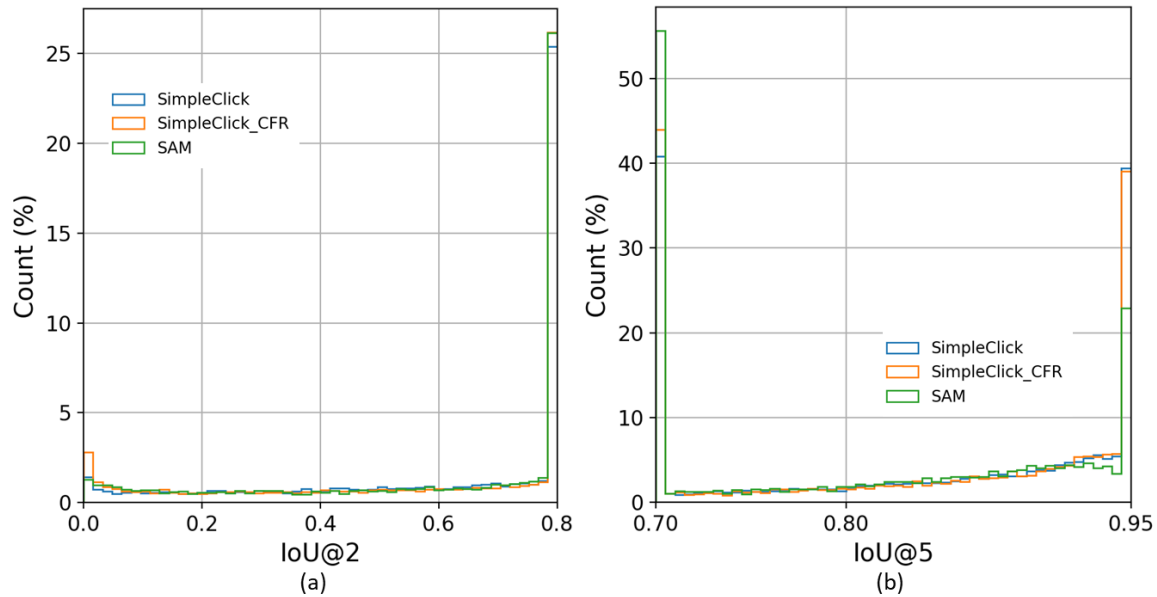


Figure 11. Histogram analysis for the segmentation results given $k = 2$ and 5.

In the SAM paper, the authors compare SAM with RITM, FocalClick, and SimpleClick, which are mentioned in this article [26]. Consistent with the conclusion drawn from Figure 11(a), SAM can achieve lower single-point performance. This indicates that when the number of clicks is limited, especially in the range of 1-5, SAM can more readily yield a relatively positive result (with an IoU exceeding 70%). However, for more refined segmentation requirements, SimpleClick/SimpleClick-CFR can more easily help the IoU to attain over 90% with more input. Given the diverse shapes of landmark objects in urban land classification, Figure 10 also hints that SAM might not excel in outlining the edges of landmark objects. This could be the reason why the classification results of SimpleClick/SimpleClick-CFR models are superior.

The demo tool provided by SAM supports several different prompts including 'point,' 'box,' 'mask,' and 'arbitrary format text'. However, in this study, we only compared the 'point' prompt mode of SAM. While SAM's model is powerful for automatic segmentation tasks, this paper specifically discusses click-based interactive segmentation models. SAM has been widely discussed recently. Therefore, our tool has also integrated the primarily click-based SAM model. At present, there are some geo-based SAM tools, such as the SAM tool of ArcGIS Pro and SAMJS developed by AntV (citation). After experiencing the demos of these tools, you will find that their interactivity is relatively poor.

5.2 Model performance on remote sensing images

One crucial aspect we explored was the impact of different band combinations on the models' performance. In particular, the inclusion of the Near-Infrared (NIR) band proved to be significant for vegetation monitoring and analysis. The NIR band captures essential information related to vegetation health, density, and other relevant parameters. Therefore, we conducted experiments using different band combinations, including RGB and RGIR, with the expectation that models trained on the PRGIR dataset would excel in segmenting trees and grass. However, the results displayed in Table 6 and Table 7 indicate that the performance of the models on both PRGB and PRGIR datasets remains comparable,

suggesting that the models can effectively handle vegetation segmentation regardless of the specific band combination. In addition to vegetation, we focused on other land cover classes such as buildings, impervious surfaces, and cars. Among these classes, buildings demonstrated the most favorable results, as their regular and well-defined shapes facilitated accurate segmentation. The models consistently performed well in segmenting buildings, indicating their ability to effectively capture the distinct characteristics of this class.

Furthermore, we extended our analysis to explore the relationship between the size of land cover objects and the models' segmentation performance. Interestingly, we observed that smaller land objects required more clicks to achieve accurate segmentation. This finding suggests that fine details and intricate structures in smaller objects necessitate additional user input for precise delineation.

By combining these findings, we can conclude that the discussed models exhibit promising performance in remote sensing applications. They showcase the ability to effectively segment various land cover classes, including vegetation and buildings, while also highlighting the influence of object size on the segmentation process. The results contribute valuable insights into the applicability and performance characteristics of these models, offering researchers and practitioners valuable guidance when applying interactive segmentation techniques to remote sensing imagery.

5.3 RSISeg tool

In the course of conducting benchmark experiments, we also developed RSISeg, an instrumental tool specifically designed for the quest of performing interactive segmentation on remote sensing data. This tool presents notable attributes, as delineated below:

1. RSISeg is explicitly engineered to facilitate the handling of remote sensing data. It is endowed with an ability to read TIFF (Tagged Image File Format) data and export GeoJson files complete with coordinates, enabling swift editing within GIS (Geographic Information Systems) software. Remote sensing imagery, often characterized by more than three spectral bands and differing satellite data types, can be seamlessly imported to the tool, and relevant parameters edited accordingly.
2. The tool offers superior interactivity compared to other interactive segmentation tools. It flourishes with features such as data window scaling, positive point-negative point addition, and retroactive deleting alterations, enriching user-software interactions significantly.
3. Furthermore, RSISeg is adept at categorizing land use and land cover in remote sensing imagery. We have pre-defined two common types duly associated with remote sensing classifications, namely, 'Trees' and 'Buildings'. Users have the liberty to add classifications as per their requirements. This tool garnishes different classifications with diverse color schemes in the results for easier deciphering. We have incorporated several models in this tool that have been proven effective in discerning remote sensing data through empirical evidence and fine-tuning. These models include SimpleClick, SimpleClick-CFR, ICL, ICL-CFR, and SAM.

Moving forward, it is envisaged to further optimize and augment this tool, making it capable of executing automated segmentation, accumulative learning, and delivering enhanced classification of land use based on remote sensing imagery.

Reference:

- [1] X. Li, W. Y. Chen, G. Sanesi, and R. Laforzezza, "Remote sensing in urban forestry: Recent applications and future directions," *Remote Sensing*, vol. 11, no. 10, p. 1144, 2019.
- [2] S. Khanal, J. Fulton, and S. Shearer, "An overview of current and potential applications of thermal remote sensing in precision agriculture," *Computers and Electronics in Agriculture*, vol. 139, pp. 22–32, 2017.
- [3] D. C. Dauwalter, K. A. Fesenmyer, R. Bjork, D. R. Leasure, and S. J. Wenger, "Satellite and airborne remote sensing applications for freshwater fisheries," *Fisheries*, vol. 42, no. 10, pp. 526–537, 2017.
- [4] L. Ma, Y. Liu, X. Zhang, Y. Ye, G. Yin, and B. A. Johnson, "Deep learning in remote sensing applications: A meta-analysis and review," *ISPRS journal of photogrammetry and remote sensing*, vol. 152, pp. 166–177, 2019.
- [5] C. K. Paul and A. C. Mascarenhas, "Remote sensing in development," *Science*, vol. 214, no. 4517, pp. 139–145, 1981.
- [6] P. Coseo and L. Larsen, "How factors of land use/land cover, building configuration, and adjacent heat sources and sinks explain Urban Heat Islands in Chicago," *Landscape and Urban Planning*, vol. 125, pp. 117–129, 2014.
- [7] K.-S. Cheng, Y.-F. Su, F.-T. Kuo, W.-C. Hung, and J.-L. Chiang, "Assessing the effect of landcover changes on air temperature using remote sensing images—A pilot study in northern Taiwan," *Landscape and Urban Planning*, vol. 85, no. 2, pp. 85–96, 2008.
- [8] G. Camps-Valls, T. V. B. Marsheva, and D. Zhou, "Semi-supervised graph-based hyperspectral image classification," *IEEE transactions on Geoscience and Remote Sensing*, vol. 45, no. 10, pp. 3044–3054, 2007.
- [9] T. Falk *et al.*, "U-Net: deep learning for cell counting, detection, and morphometry," *Nature methods*, vol. 16, no. 1, pp. 67–70, 2019.
- [10] N. Kussul, M. Lavreniuk, S. Skakun, and A. Shelestov, "Deep Learning Classification of Land Cover and Crop Types Using Remote Sensing Data," *IEEE Geoscience and Remote Sensing Letters*, vol. 14, no. 5, pp. 778–782, May 2017, doi: 10.1109/LGRS.2017.2681128.
- [11] H. Huang, Y. Lan, A. Yang, Y. Zhang, S. Wen, and J. Deng, "Deep learning versus Object-based Image Analysis (OBIA) in weed mapping of UAV imagery," *International Journal of Remote Sensing*, vol. 41, no. 9, pp. 3446–3479, 2020.
- [12] G. Cheng, X. Xie, J. Han, L. Guo, and G.-S. Xia, "Remote sensing image scene classification meets deep learning: Challenges, methods, benchmarks, and opportunities," *IEEE Journal of Selected Topics in Applied Earth Observations and Remote Sensing*, vol. 13, pp. 3735–3756, 2020.
- [13] W.-D. Jang and C.-S. Kim, "Interactive Image Segmentation via Backpropagating Refinement Scheme," in *Proceedings of the IEEE/CVF Conference on Computer Vision and Pattern Recognition*, 2019, pp. 5297–5306.
- [14] S. Zhang, J. H. Liew, Y. Wei, S. Wei, and Y. Zhao, "Interactive object segmentation with inside-outside guidance," in *Proceedings of the IEEE/CVF conference on computer vision and pattern recognition*, 2020, pp. 12234–12244.
- [15] M. D. Hossain and D. Chen, "Segmentation for Object-Based Image Analysis (OBIA): A review of algorithms and challenges from remote sensing perspective," *ISPRS Journal of Photogrammetry and Remote Sensing*, vol. 150, pp. 115–134, 2019.
- [16] G. M. Espindola, G. Câmara, I. A. Reis, L. S. Bins, and A. M. Monteiro, "Parameter selection for region-growing image segmentation algorithms using spatial autocorrelation," *International Journal of Remote Sensing*, vol. 27, no. 14, pp. 3035–3040, 2006.
- [17] M. Ferecatu and N. Boujemaa, "Interactive remote-sensing image retrieval using active relevance feedback," *IEEE Transactions on Geoscience and Remote Sensing*, vol. 45, no. 4, pp. 818–826, 2007.

- [18] L. Ge, R. Ju, T. Ren, and G. Wu, "Interactive RGB-D Image Segmentation Using Hierarchical Graph Cut and Geodesic Distance," in *Advances in Multimedia Information Processing -- PCM 2015*, Y.-S. Ho, J. Sang, Y. M. Ro, J. Kim, and F. Wu, Eds., in Lecture Notes in Computer Science. Cham: Springer International Publishing, 2015, pp. 114–124. doi: 10.1007/978-3-319-24075-6_12.
- [19] T. Kattenborn, J. Leitloff, F. Schiefer, and S. Hinz, "Review on Convolutional Neural Networks (CNN) in vegetation remote sensing," *ISPRS journal of photogrammetry and remote sensing*, vol. 173, pp. 24–49, 2021.
- [20] Z. Li *et al.*, "Deep Learning-Based Object Detection Techniques for Remote Sensing Images: A Survey," *Remote Sensing*, vol. 14, no. 10, p. 2385, 2022.
- [21] T. Portenier, Q. Hu, A. Szabo, S. A. Bigdeli, P. Favaro, and M. Zwicker, "Faceshop: Deep sketch-based face image editing," *arXiv preprint arXiv:1804.08972*, 2018.
- [22] K. Suzuki, "Overview of deep learning in medical imaging," *Radiological physics and technology*, vol. 10, no. 3, pp. 257–273, 2017.
- [23] K. Sofiiuk, I. Petrov, O. Barinova, and A. Konushin, "f-brs: Rethinking backpropagating refinement for interactive segmentation," in *Proceedings of the IEEE/CVF Conference on Computer Vision and Pattern Recognition*, 2020, pp. 8623–8632.
- [24] S. Sun, M. Xian, F. Xu, T. Yao, and L. Capriotti, "CFR-ICL: Cascade-Forward Refinement with Iterative Click Loss for Interactive Image Segmentation," *arXiv preprint arXiv:2303.05620*, 2023.
- [25] X. Chen, Z. Zhao, Y. Zhang, M. Duan, D. Qi, and H. Zhao, "FocalClick: Towards Practical Interactive Image Segmentation," in *Proceedings of the IEEE/CVF Conference on Computer Vision and Pattern Recognition*, 2022, pp. 1300–1309.
- [26] A. Kirillov *et al.*, "Segment anything," *arXiv preprint arXiv:2304.02643*, 2023.
- [27] Q. Liu, Z. Xu, G. Bertasius, and M. Niethammer, "SimpleClick: Interactive Image Segmentation with Simple Vision Transformers," Nov. 2022.
- [28] A. P. Tewkesbury, A. J. Comber, N. J. Tate, A. Lamb, and P. F. Fisher, "A critical synthesis of remotely sensed optical image change detection techniques," *Remote Sensing of Environment*, vol. 160, pp. 1–14, 2015.
- [29] R. Buitenwerf, L. Rose, and S. I. Higgins, "Three decades of multi-dimensional change in global leaf phenology," *Nature Climate Change*, vol. 5, no. 4, p. 364, 2015.
- [30] N. Audebert, B. L. Saux, and S. Lefèvre, "Semantic Segmentation of Earth Observation Data Using Multimodal and Multi-scale Deep Networks," *arXiv:1609.06846 [cs]*, Sep. 2016, Accessed: Aug. 09, 2020. [Online]. Available: <http://arxiv.org/abs/1609.06846>
- [31] B. Demir, F. Bovolo, and L. Bruzzone, "Updating land-cover maps by classification of image time series: A novel change-detection-driven transfer learning approach," *IEEE Transactions on Geoscience and Remote Sensing*, vol. 51, no. 1, pp. 300–312, 2012.
- [32] J. A. dos Santos, P.-H. Gosselin, S. Philipp-Foliguet, R. da S. Torres, and A. X. Falcão, "Interactive Multiscale Classification of High-Resolution Remote Sensing Images," *IEEE Journal of Selected Topics in Applied Earth Observations and Remote Sensing*, vol. 6, no. 4, pp. 2020–2034, Aug. 2013, doi: 10.1109/JSTARS.2012.2237013.
- [33] B. Demir, C. Persello, and L. Bruzzone, "Batch-Mode Active-Learning Methods for the Interactive Classification of Remote Sensing Images," *IEEE Transactions on Geoscience and Remote Sensing*, vol. 49, no. 3, pp. 1014–1031, Mar. 2011, doi: 10.1109/TGRS.2010.2072929.
- [34] H. Hichri, Y. Bazi, N. Alajlan, and S. Malek, "Interactive segmentation for change detection in multispectral remote-sensing images," *IEEE Geoscience and Remote Sensing Letters*, vol. 10, no. 2, pp. 298–302, 2012.
- [35] P. M. Dare, "Shadow analysis in high-resolution satellite imagery of urban areas," *Photogrammetric Engineering & Remote Sensing*, vol. 71, no. 2, pp. 169–177, 2005.

- [36] "Vaihingen 2D Semantic Labeling - ISPRS."
<http://www2.isprs.org/commissions/comm2/wg4/vaihingen-2d-semantic-labeling-contest.html>
(accessed Jun. 09, 2020).
- [37] Z. Wang, C. Fan, and M. Xian, "Application and Evaluation of a Deep Learning Architecture to Urban Tree Canopy Mapping," *Remote Sensing*, vol. 13, no. 9, Art. no. 9, Jan. 2021, doi: 10.3390/rs13091749.
- [38] K. Sofiuk, I. A. Petrov, and A. Konushin, "Reviving Iterative Training with Mask Guidance for Interactive Segmentation," in *2022 IEEE International Conference on Image Processing (ICIP)*, Oct. 2022, pp. 3141–3145. doi: 10.1109/ICIP46576.2022.9897365.
- [39] S. Nowozin, "Optimal decisions from probabilistic models: the intersection-over-union case," in *Proceedings of the IEEE conference on computer vision and pattern recognition*, 2014, pp. 548–555.
- [40] Q. Weng, "Remote sensing of impervious surfaces in the urban areas: Requirements, methods, and trends," *Remote Sensing of Environment*, vol. 117, pp. 34–49, 2012.